IEEE Photonics Journal
An IEEE Photonics Society Publication

Open Access

High-Sensitivity Sensing Based on Plasmon-Induced Transparency

Volume 7, Number 5, October 2015

B. X. Li
H. J. Li
L. L. Zeng
S. P. Zhan
Z. H. He
Z. Q. Chen
H. Xu

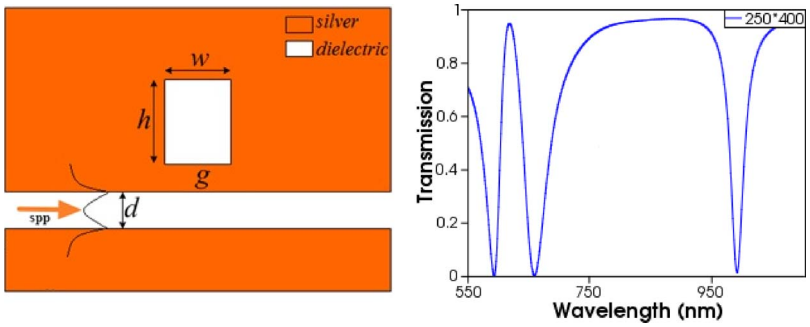

DOI: 10.1109/JPHOT.2015.2483202
1943-0655

IEEE photonics SOCIETY

IEEE

High-Sensitivity Sensing Based on Plasmon-Induced Transparency

B. X. Li,[1] H. J. Li,[1] L. L. Zeng,[2] S. P. Zhan,[1] Z. H. He,[1] Z. Q. Chen,[1] and H. Xu[1]

[1]College of Physics and Electronics, Central South University, Changsha 410083, China.
[2]College of Solar Energy Engineering, Hunan Vocational Institute of Technology, Xiangtan 411104, China.

DOI: 10.1109/JPHOT.2015.2483202

Manuscript received September 11, 2015; revised September 22, 2015; accepted September 24, 2015. Date of publication October 1, 2015; date of current version October 13, 2015. This work was supported in part by the Research Fund for the Doctoral Program of Higher Education of China under Grant 20100162110068 and in part by the National Natural Science Foundation of China under Grant 61275174. Corresponding author: H. J. Li (e-mail: lihj398@126.com).

Abstract: High-sensitivity sensing based on plasmon-induced transparency (PIT) in a rectangular resonator has been investigated in detail. Multimode theory is introduced to explain the redshift and blueshift of the transmission spectrum by adjusting a structural parameter (w or h). In sensing applications, the sensitivity of the proposed structure is about 800 nm/RIU, and its figure of merit (FOM) is as high as 17280. In addition, the influences of structural parameters on FOM are researched in detail. The results indicate that structural parameters play important roles in optimizing the sensing performance, and the length (h) is more sensitive than the width (w) for FOM. The plasmonic configuration has the advantages of easy fabrication and compactness, which may find important applications in highly integrated optics devices, optical communication, and sensitive nanometer-scale refractive index sensors.

Index Terms: High-sensitivity sensing, plasmonics, waveguide, plasmon-induced transparency (PIT).

1. Introduction

Electromagnetically induced transparency (EIT), which occurs in atomic systems, arises from quantum interference between the atomic resonances [1]. Due to the wide applications in slow light, nonlinear optics, quantum information processing, optical data storage, and biosensor [2]–[4], EIT has attracted considerable attention in recent decades. However, the strict restrictions on the realization of EIT hinder its practical application. Surface plasmon polaritons (SPPs) which are trapped on the metal–insulator interface have the capabilities to overcome the classical diffraction limit and manipulate light in the nanoscale domain [5]–[7]. Plasmon-induced transparency (PIT) is a plasmonic analog of the EIT. A number of devices based on SPPs have been numerically simulated and experimentally demonstrated, such as bandpass filter, sensors, optical buffers, and amplifiers [8]–[11]. Among these devices, metal–dielectric–metal (MDM) waveguides are the most promising for realization of nanoscale devices, owing to their deep-subwavelength confinement of light and relatively easy fabrication [12]–[17].

In past years, PIT based on MDM waveguide have been theoretically predicted and experimentally demonstrated in previous literatures [13], [14], [18]–[22]. Lu *et al.* established

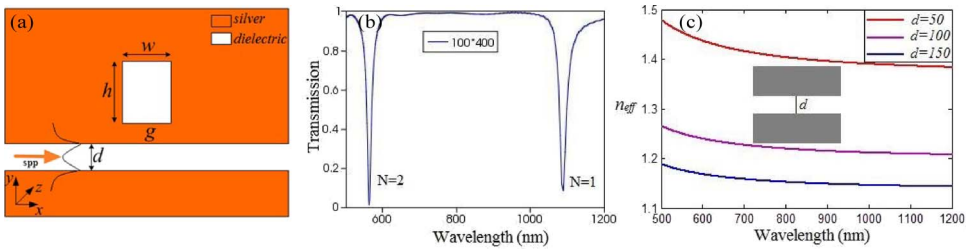

Fig. 1. (a) Schematic diagram of the individual rectangular resonator coupled with MDM waveguide. (b) Transmission spectrum with $w = 100$ nm and $h = 400$ nm. (c) Effective refractive index with different width as a function of wavelength. d and g are fixed to 50 nm and 15 nm, respectively.

multi-nanoresonator-coupled waveguide systems to study PIT theoretically [14]. Zhan *et al.* researched the PIT based on ring-resonators coupled channel drop filter systems [19]. A chip-integrated multichannel filter was constructed to study PIT experimentally [22]. PIT can be observed in two structures with different and identical dimension [12], [14], [17]–[20], [23], [24]. Some literatures reported that PIT can be realized in single microdisk, whispering-gallery and stub resonator [25]–[27]. In recent years, plasmonic sensor is of great importance for device applications. Plasmonic sensors based on various structures have been investigated numerically and theoretically, such as cavity, stub, ring, asymmetric and terminal closed T-shaped and so on [28]–[32]. Due to the steeper variation in optical spectrum and slow-light, the PIT sensor performance is better than the non-PIT one [32].

In this paper, high sensitivity sensing based on PIT in a rectangular resonator coupled with bus waveguide has been investigated in detail. Due to the destructive interference between resonance modes, PIT can be observed. The finite-difference time-domain (FDTD) with perfectly matched layer (PML) absorbing boundary is introduced to investigate the configuration. Multimode theory is introduced to explain the redshift and blueshift of transmission spectrum by adjusting a structural parameter (w or h). The plasmonic nano sensor has a sensitivity of 800 nm/RIU and a FOM of 17280. It is found that structural parameters play important roles in optimizing the sensing performance. The finds have potential applications in the on chip nano sensing.

2. Model

The proposed structure is schematically shown in Fig. 1(a), consisting of a bus waveguide coupled with a rectangular resonator. The width of bus waveguide and rectangular resonator are respectively set to be d and w. h denotes the length of rectangular resonator. g stands for the distance between bus waveguide and rectangular resonator. The orange–red area is silver, whose complex relative permittivity is characterized by Drude model $\varepsilon_m(\omega) = \varepsilon_\infty - \omega_p/(\omega^2 + i\omega\gamma_p)$, where the dielectric constant $\varepsilon_\infty = 3.7$ at the infinite frequency, the bulk plasma frequency $\omega_p = 1.38 \times 10^{16}$ rad/s, ω stands for the angle frequency of incident wave, the damping rate $\gamma_p = 2.73 \times 10^{13}$ rad/s characters as the absorption loss [33].

3. Results and Discussion

The transmission spectrum with $w = 100$ nm and $h = 400$ nm is shown in Fig. 1(b), which clearly shows two resonance dips. In this paper, d and g are fixed to 50 nm and 15 nm, respectively. Based on Coupled Mode Theory (CMT), we define ϕ to be the phase delay per round-trip in the rectangular resonator, one has $\phi = 4\pi n_{\text{eff}} H/\lambda + \phi_r$, where ϕ_r is the phase shift of a beam reflected on the upper and lower (left and right) facets of the resonator, H presents the h or w of the rectangular cavity [34], n_{eff} is the effective refractive index which can be obtained by the dispersion equation [14]

$$\varepsilon_m \sqrt{n_{\text{eff}}^2 - \varepsilon_d} \tanh\left(\frac{d\pi\sqrt{n_{\text{eff}}^2 - \varepsilon_d}}{\lambda}\right) + \varepsilon_d \sqrt{n_{\text{eff}}^2 - \varepsilon_m} = 0 \quad (1)$$

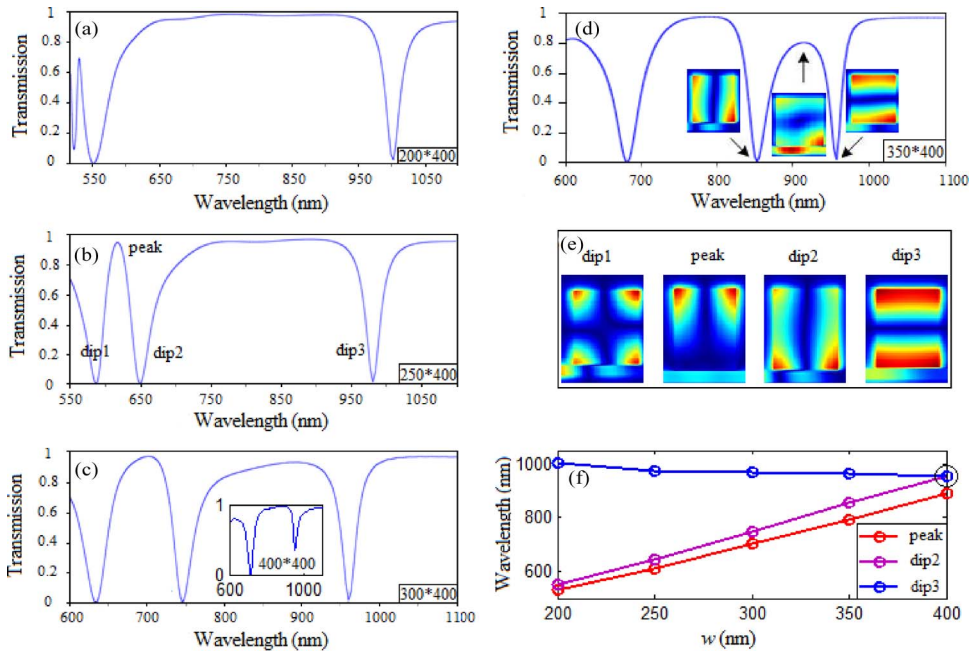

Fig. 2. Transmission spectra with $w = 200$ nm (a), 250 nm (b), 300 nm (c), 350 nm (d), and $h = 400$ nm, respectively. (e) The magnetic field distributions of dip1/peak/dip2/dip3 in Fig. 3(b). (f) The wavelength shift of peak/dip2/dip3 against the change of w with a step of 50 nm.

where ε_m and ε_d stand for the dielectric constant of metal and dielectric waveguide with a width of d, respectively. To simplify the calculation, the dielectric is set to be air $(\varepsilon_d = 1)$. According to equation (1), the effective index n_{eff} with different width for wavelength ranging from 500 nm to 1200 nm are plotted in Fig. 1(c). When resonant condition is satisfied $(\phi = N \cdot 2\pi)$, where N is positive integer and corresponds to the order of the resonant mode, the resonant wavelength can be expressed as $\lambda_m = 2n_{\text{eff}}H/(N - \phi_r/2\pi)$. Thus, the two resonance dips in Fig. 1(b) are respectively the first-order mode and the second-order one.

Fig. 2(a)–(d) respectively display the transmission spectra with various w and $h = 400$ nm. Interestingly, when w equals to 200 nm, a typical PIT can be observed, where a transparency peak at 531 nm is located between two dips at 522.5 nm and 554 nm. According to Fig. 1(b), we consider that the transparency window can be regarded as the splitting of the second-order mode. As the w continues to increase, the transparency window shows redshift together with an enhanced transmittance.

As reported in Ref. [27], when the rectangular cavity is big enough, the x- and y-directional resonances can be excited in the cavity. The resonance modes are denoted by TM_{mn}, where m and n denote the number of node of standing waves in horizontal and vertical directions in the rectangular cavity. In order to understand the underlying physics of the resonant modes in the transmission spectrum, the corresponding magnetic field intensity $|H_z|$ for the transmission peak and dips are displayed in Fig. 2(e) when $w = 250$ nm and $h = 400$ nm. And the resonance modes can be expressed as TM_{11}, TM_{10}, TM_{10} and TM_{01}, respectively. Therefore, the PIT optical response in this proposed structure can be ascribed to the destructive interference between resonance modes (TM_{11} and TM_{10}), which is similar to the formation mechanisms of PIT in previous work [27]. Likewise, due to the destructive interference between TM_{10} and TM_{01}, PIT can be observed in Fig. 2(d).

Fig. 2(f) shows the wavelength shift of peak/dip2/dip3 against the change of w with a step of 50 nm. With the increasing of w, dip2 and peak rise monotonously and shift to longer wavelength. On the contrary, dip3 shifts to shorter wavelength. As the peak shifts to longer wavelength, the

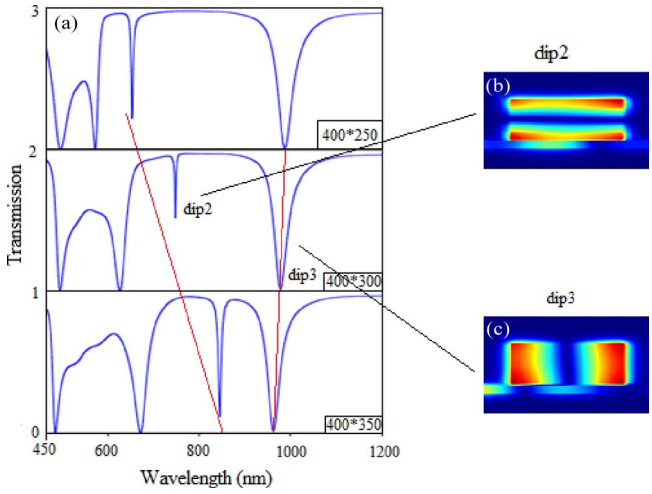

Fig. 3. (a) Transmission spectra with different h and $w = 400$ nm. (b) and (c) are, respectively, the magnetic field distributions of dip2 and dip3.

transmission intensity between dip2 and dip3 becomes increasingly smaller. Finally, dip2 and dip3 overlap at the wavelength of 956 nm when $w = 400$ nm, as shown in the inset of Fig. 2(c).

As described above, increasing w will give rise to two opposite results: One is the redshift of dip2 (peak), and the other is the blueshift of dip3. Then, how to explain the counterintuitive phenomenon? As illustrated in Fig. 2(e), the resonance modes of peak, dip2 and dip3 are denoted TM_{10}, TM_{10} and TM_{01}, respectively. According to the results of Ref. [34], when the magnetic field is vertical symmetry (peak, dip2), the length of resonator equals to w $(H = w)$. On the contrary, when the magnetic field is horizontal symmetry (dip3), the width of resonator is w and the length of resonator equals to h $(H = h)$. Based on $\lambda_m = 2n_{\text{eff}}H/(N - \phi_r/2\pi)$, it is concluded that increasing w can generate two consequences, the one is increasing the effective length of resonator (just as the case of peak and dip2) which gives rise to the increasing of the resonant wavelength, and the other is increasing the width of resonator (just as the case of dip3) which leads to the decreasing of refractive index and resonant wavelength.

Can the theory be applied to the other case? The transmission spectra with different h are depicted in Fig. 3(a). Obviously, the change tendencies of dip2/dip3 are the same as that in Fig. 2(f). Fig. 3(b) and (c) displays the magnetic field distributions of dip2 and dip3 with $w = 400$ nm and $h = 300$ nm. Just as shown in Fig. 3(b), the magnetic field of dip2 is horizontal symmetry, which means the length of resonator equals to h $(H = h)$. Analogously, the magnetic filed of dip3 is vertical symmetry, which means the width of resonator equals to h. In other words, increasing h stands for increasing the length of resonator (redshift) for dip2 while increasing the width of resonator (blueshift) for dip3. In summary, the theory can also be suitable for the case of changing h in rectangular resonator. It is worthwhile to mention that the wavelength shift of dip3 is less than that of dip2/peak, which is attributed to the fact that the variation of n_{eff} is very small by changing the width of waveguide. As far as we know, there are few studies on PIT based on an individual rectangular resonator coupled with bus waveguide. The simple structure possesses the advantage of easy fabrication and compactness, which has potential applications in optical data storage, highly integrated optical circuits and optical buffers.

As a research hotspot, the sensor has attracted great interests, and PIT is considered to be very sensitive to the surround environment variation and can be applied in sensor. As an important index in sensor, the $Sensivity = \Delta\lambda/\Delta n$, where $\Delta\lambda$ *and* Δn respectively stand for spectrum shift and the change of the effective refractive index, is introduced to characterize the sensor performance. Fig. 4(a) shows the transmission spectra with the parameters of $w = 350$ nm, $h = 400$ nm for the change of refractive indices from 1 to 1.04 with a step of 0.01.

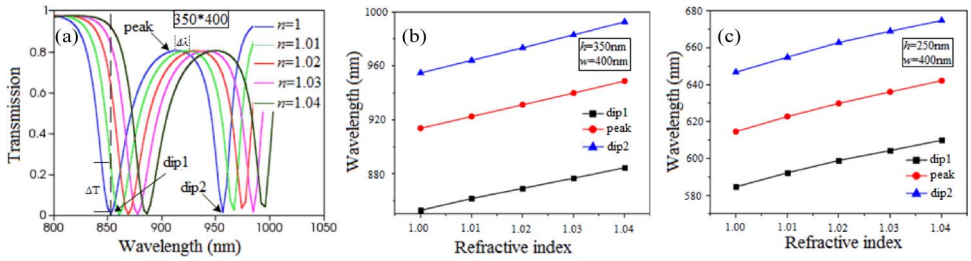

Fig. 4. (a) Transmission spectra with $w = 350$ nm, $h = 400$ nm for the change of refractive indices with a step of 0.01. (b) and (c) Wavelength of dip1/dip2/peak shift against refractive indices when $w = 350$ nm and 250 nm.

As shown in Fig. 4(b), when the environment (dielectric) refractive index increases, a clear redshift of the spectrum is visible, and the peak wavelength shifts from 916.8 nm to 924.7 nm and then to 949 nm as refractive index n_{eff} increases from 1 to 1.01 and then to 1.04. Similarly, the dip1/dip2 almost increases linearly with the increasing of refractive index. The slopes of dip1/dip2/peak are almost equivalent. The sensitivity is about 800 nm/RIU from Fig. 4(b). Fig. 4(c) shows the wavelength of dip1/dip2/peak shift against refractive indices when $w = 250$ nm, $h = 400$ nm. It is concluded from Fig. 4(c) that the sensitivity is about 590 nm/RIU when $w = 250$ nm, $h = 400$ nm, which is lower than that when $w = 350$ nm, $h = 400$ nm. According to the linear relationship between the wavelength shift and the refractive index, detecting the wavelength shift of the transmission spectrum can obtain the refractive index of the material under sensing, which is the sensing principle of the proposed device. In this regard, the high sensitivity is beneficial to sensor. As far as we know, the sensitivity of the proposed structure is higher than previous reports [35]–[38].

The figure of merit (FOM), as another key factor of the sensor, is introduced to evaluate the performance of the sensor and studied in detail. Considering that lasers are widely used in practice (one wavelength output), a FOM at a fixed wavelength can be defined as $\text{FOM} = |(\Delta T/\Delta n)/T|$ [39], where T is the transmittance at the specific wavelength, $\Delta T/\Delta n$ is the transmittance change at fixed wavelength induced by a refractive index change, which are respectively denoted in Fig. 4(a). According to the definition of FOM, it can predict that a larger FOM can be obtained by an ultra-low transmittance and a sharp change of transmittance induced by the index changes. Fig. 5(a) shows the FOM and the corresponded transmission spectrum with $w = 350$ nm, $h = 400$ nm and $n = 1.01$. It is found that the maximum FOM nearly appears at the transmission dips, which is attributed to the lowest initial intensity T here, and the corresponded maximum FOM of dip1 and dip2 are 4259 and 1566, respectively.

In order to study the maximum FOM well, we research the effect of various w and h on FOM in detail. Fig. 5(b) describes the maximum FOM of dip1/dip2 against different h ($w = 400$ nm, $d = 50$ nm, $g = 15$ nm). The results reveal that the maximum FOM of dip1 decreases monotonously from 17280 to 1600 when h increases from 200 nm to 375 nm. However, the maximum FOM of dip2 first decreases from 4468 to 83 and then increases to 1489 when h increases from 200 nm to 300 nm and then to 375 nm. Fig. 5(c) displays the maximum FOM with different w ($h = 400$ nm, $d = 50$ nm, $g = 15$ nm). Different from the influence of adjusting h on FOM, the variation tendencies of dip1 and dip2 are similar. The maximum FOM of dip1 and dip2 can be obtained when w increases to 250 nm. When the w is greater or less than 250 nm, the maximum FOM will decrease distinctly. What is noteworthy is that and the length (h) is more sensitive than the width (w) for FOM.

At last, the influence of different distance g on the maximum FOM at dip1 and dip2 ($w = 350/250$ nm and $h = 400$ nm) are investigated in detail and shown in Fig. 5(d) and (e), respectively. Obviously, it can be seen from Fig. 5(d) that the maximum FOM of dip1 achieves the maximum when distance (g) increases to 15 nm. As g continues to increase, the FOM shows a monotonic decrease. On the contrary, the maximum FOM of dip2 decreases monotonously and

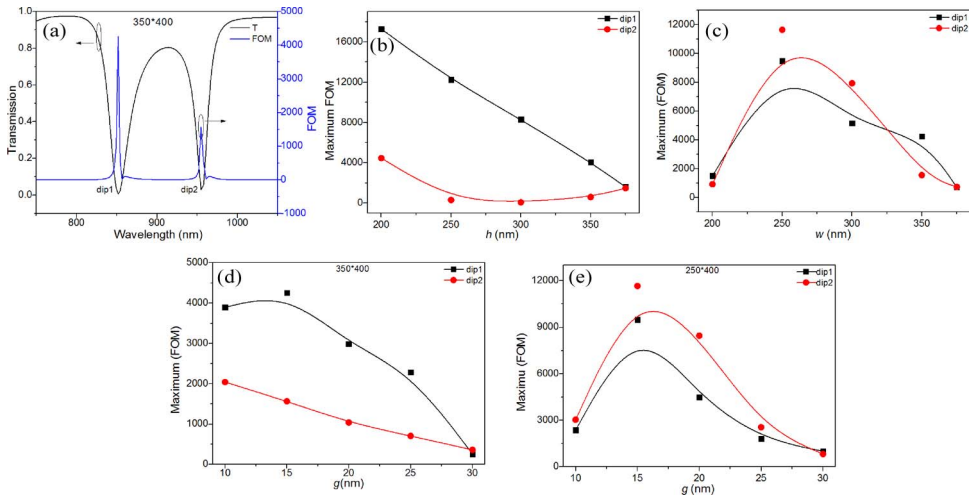

Fig. 5. (a) Transmission spectrum and FOM with $w = 350$ nm, $h = 400$ nm, and $n_{\text{eff}} = 1.01$. (b) and (c) Maximum FOM against different h ($w = 400$ nm) and w ($h = 400$ nm) at dip1 and dip2. (d) and (e) Influence of different distance g on the maximum FOM at dip1 and dip2 when $w = 350$ nm, $h = 400$ nm and $w = 250$ nm, $h = 400$ nm.

manifests a linear relation with g. It is found that the variation tendencies of dip1 and dip2 are similar when $w = 250$ nm and $h = 400$ nm from Fig. 5(e). The FOM achieves the maximum when g equals to 15 nm, and the maximum FOM will reduce when g is greater or less than 15 nm. In summary, the structural parameters play important roles in optimizing the sensing performance.

4. Conclusion

To sum up, high sensitivity sensing based on PIT in a rectangular resonator coupled with bus waveguide has been investigated in detail. Due to the destructive interference between resonance modes, PIT can be observed. Multi-mode theory is introduced to explain the redshift and blueshift of transmission spectrum by adjusting a structural parameter. The plasmonic nano sensor has a sensitivity of 800 nm/RIU and a FOM of 17280. It is found that structural parameters play important roles in optimizing the sensing performance. Because of easy fabrication and compactness, the structure has potential applications in highly integrated optics devices and plasmonic nano-sensing area.

References

[1] M. Fleischhauer, A. Imamoglu, and J. Marangos, "Electromagnetically induced transparency: Optics in coherent media," *Rev. Mod. Phys.*, vol. 77, no. 2, pp. 633–673, Jul. 2005.
[2] I. Novikova, R. Walsworth, and Y. Xiao, "Electromagnetically induced transparency-based slow and stored light in warm atoms," *Laser Photon. Rev.*, vol. 6, no. 3, pp. 333–353, May 2012.
[3] X. Yang, S. Li, C. Zhang, and H. Wang, "Enhanced cross-Kerr nonlinearity via electromagnetically induced transparency in a four-level tripod atomic system," *J. Opt. Soc. Amer. B*, vol. 26, no. 7, pp. 1423–1434, Dec. 2009.
[4] R. Beausoleil, W. Munro, D. Rodrigues, and T. Spiller, "Applications of electromagnetically induced transparency to quantum information processing," *J. Mod. Opt.*, vol. 51, no. 16, pp. 2441–2448, Dec. 2004.
[5] W. Barnes, A. Dereux, and T. Ebbesen, "Review article surface plasmon subwavelength optics," *Nature*, vol. 424, no. 6950, pp. 824–830, Aug. 2003.
[6] S. Bozhevolnyi, V. Volkov, E. Devaux, J. Laluet, and T. Ebbesen, "Channel plasmon subwavelength waveguide components including interferometers and ring resonators," *Nature*, vol. 440, no. 7083, pp. 508–511, Jan. 2006.
[7] Q. Gan, Y. Gao, Q. Wang, L. Zhu, and F. Bartoli, "Surface plasmon waves generated by nanogrooves through spectral interference," *Phys. Rev. B.*, vol. 81, no. 8, Feb. 2010, Art. ID. 085443.
[8] H. Lu, X. Liu, L. Wang, Y. Gong, and D. Mao, "Ultrafast all-optical switching in nanoplasmonic waveguide with Kerr nonlinear resonator," *Opt. Exp.*, vol. 19, no. 4, pp. 2910–2915, Feb. 2011.
[9] D. Oosten, M. Spasenović, and L. Kuipers, "Nanohole chains for directional and localized surface plasmon excitation," *Nano Lett.*, vol. 10, no. 1, pp. 286–290, Jan. 2010.

[10] Q. Gan, Y. Ding, and F. Bartoli, "'Rainbow' trapping and releasing at telecommunication wavelengths," *Phys. Rev. Lett.*, vol. 102, no. 5, Feb. 2009, Art. ID. 056801.
[11] J. Park, H. Kim, and B. Lee, "High order plasmonic Bragg reflection in the metal–insulator–metal waveguide Bragg grating," *Opt. Exp.*, vol. 16, no. 1, pp. 413–425, Jan. 2008.
[12] B. Li *et al.*, "Tunable filter and optical buffer based on dual plasmonic ring resonators," *J. Mod. Opt.*, vol. 62, no. 3, pp. 212–220, Feb. 2015.
[13] Z. Zhang, L. Zhang, H. Li, and H. Chen, "Plasmon induced transparency in a surface plasmon polariton waveguide with a comb line slot and rectangle cavity," *Appl. Phys. Lett.*, vol. 104, no. 23, Jun. 2014, Art. ID. 231114.
[14] H. Lu, X. Liu, and D. Mao, "Plasmonic analog of electromagnetically induced transparency in multi-nanoresonator-coupled waveguide systems," *Phys. Rev. A*, vol. 85, no. 5, May 2012, Art. ID. 053803.
[15] I. Zand, M. Abrishamian, and P. Berini, "Highly tunable nanoscale metal–insulator–metal Split Ring Core Ring Resonators (SRCRRs)," *Opt. Exp.*, vol. 21, no. 1, pp. 79–86, Jan. 2013.
[16] J. Chen, C. Sun, and Q. Gong, "Fano resonances in a single defect nanocavity coupled with a plasmonic waveguide," *Opt. Lett.*, vol. 39, no. 1, pp. 52–55, Jan. 2014.
[17] G. Cao *et al.*, "Uniform theoretical description of plasmon-induced transparency in plasmonic stub waveguide," *Opt. Lett.*, vol. 39, no. 2, pp. 216–219, Jan. 2014.
[18] Z. He, H. Li, S. Zhan, G. Cao, and B. Li, "Combined theoretical analysis for plasmon-induced transparency in waveguide systems," *Opt. Lett.*, vol. 39, no. 19, pp. 5543–5546, Oct. 2014.
[19] S. Zhan *et al.*, "Theoretical analysis of plasmon-induced transparency in ring-resonators coupled channel drop filter systems," *Plasmonics*, vol. 9, no. 6, pp. 1431–1437, Dec. 2014.
[20] G. Cao *et al.*, "Formation and evolution mechanisms of plasmon-induced transparency in MDM waveguide with two stub resonators," *Opt. Exp.*, vol. 21, no. 8, pp. 9198–9205, Apr. 2013.
[21] R. Kekatpure, E. Barnard, W. Cai, and M. Brongersma, "Phase-coupled plasmon-induced transparency," *Phys. Rev. Lett.*, vol. 104, no. 24, Jun. 2010, Art. ID. 243902.
[22] X. Yang *et al.*, "Tunable ultracompact chip-integrated multichannel filter based on plasmon-induced transparencies," *Appl. Phys. Lett.*, vol. 104, no. 22, Jun. 2014, Art. ID. 221114.
[23] Z. Liu *et al.*, "PIT-like effect in asymmetric and symmetric C-shaped metamaterials," *Opt. Mater.*, vol. 35, no. 5, pp. 948–953, Mar. 2013.
[24] S. Zhan *et al.*, "Analogy of plasmon induced transparency in detuned U-resonators coupling to MDM plasmonic waveguide," *Solid State Commun.*, vol. 174, no. 11, pp. 50–54, Nov. 2013.
[25] Q. Huang *et al.*, "Electromagnetically induced transparency-like effect in a two-bus waveguides coupled microdisk resonator," *Opt. Exp.*, vol. 22, no. 3, pp. 3219–3227, Feb. 2014.
[26] B. Li *et al.*, "Experimental observation of Fano resonance in a single whispering-gallery microresonator," *Appl. Phys. Lett.*, vol. 98, no. 2, May 2011, Art. ID. 021116.
[27] G. Cao *et al.*, "Plasmon-induced transparency in a single multimode stub resonator," *Opt. Exp.*, vol. 22, no. 21, pp. 25215–25223, Oct. 2014.
[28] H. Lu, X. Liu, D. Mao, and G. Wang, "Plasmonic nanosensor based on Fano resonance in waveguide-coupled resonators," *Opt. Lett.*, vol. 37, no. 18, pp. 3780–3782, Sep. 2012.
[29] J. Chen *et al.*, "Coupled-resonator-induced Fano resonances for plasmonic sensing with ultra-high figure of merits," *Plasmonics*, vol. 8, no. 4, pp. 1627–1631, May 2013.
[30] T. Wu *et al.*, "The sensing characteristics of plasmonic waveguide with a ring resonator," *Opt. Exp.*, vol. 22, no. 7, pp. 7669–7677, Apr. 2014.
[31] X. Shang *et al.*, "Realizing Fano-like resonance in a one terminal closed T-shaped waveguide," *Eur. Phys. J. B.*, vol. 88, no. 144, pp. 1–5, Jun. 2015.
[32] J. Chen, Z. Li, S. Yue, J. Xiao, and Q. Gong, "Plasmon-induced transparency in asymmetric T-shape slit," *Nano Lett.*, vol. 12, no. 5, pp. 2494–2498, May 2012.
[33] E. D. Palik, *Handbook of Optical Constants in Solids*. Boston, MA, USA: Academic, 1982.
[34] Z. Chen and L. Yu, "Multiple Fano resonances based on different waveguide modes in a symmetry breaking plasmonic system," *IEEE Photon. J.*, vol. 6, no. 6, Dec. 2014, Art. ID. 4802208.
[35] S. Raza, G. Toscano, A. Jauho, N. Mortensen, and M. Wubs, "Refractive-index sensing with ultrathin plasmonic nanotubes," *Plasmonics*, vol. 8, no. 2, pp. 193–199, Jun. 2013.
[36] B. Gallinet and O. Martin, "Refractive index sensing with subradiant modes: A framework to reduce losses in plasmonic nanostructures," *Amer. Chem. Soc. Nano*, vol. 7, no. 8, pp. 6978–6987, Aug. 2013.
[37] K. Lodewijks *et al.*, "Tuning the Fano resonance between localized and propagating surface plasmon resonances for refractive index sensing applications," *Plasmonics*, vol. 8, no. 3, pp. 1379–1385, Nov. 2013.
[38] E. Velichko and A. Nosich, "Refractive-index sensitivities of hybrid surface-plasmon resonances for a core–shell circular silver nanotube sensor," *Opt. Lett.*, vol. 38, no. 23, pp. 4978–4981, Dec. 2013.
[39] K. Wen *et al.*, "Fano resonance with ultra-high figure of merits based on plasmonic metal–insulator–metal waveguide," *Plasmonics*, vol. 10, no. 1, pp. 27–32, Feb. 2015.